Journal of
Synchrotron
Radiation

ISSN 1600-5775

Received 22 December 2013
Accepted 10 April 2014

Energy-resolved electron-yield XAS studies of nanoporous CoAlPO-18 and CoAlPO-34 catalysts

Vladimir Martis,[a,b] Martin Martis,[b] John Lipp,[c] Dirk Detollenaere,[a] Trevor Rayment,[c] Gopinathan Sankar[b] and Wim Bras[a]*

[a]Netherlands Organization for Scientific Research (NWO), DUBBLE@ESRF, BP 220, 6 Rue Jules Horowitz, 38043 Grenoble, France, [b]Department of Chemistry, University College London, 20 Gordon Street, London WC1H 0AJ, UK, and [c]STFC Rutherford Appleton Laboratory, Harwell, Didcot OX11 0QX, UK. *E-mail: wim.bras@esrf.eu

Energy-resolved electron-yield X-ray absorption spectroscopy is a promising technique for probing the near-surface structure of nanomaterials because of its ability to discriminate between the near-surface and bulk of materials. So far, the technique has only been used in model systems. Here, the local structural characterization of nanoporous cobalt-substituted aluminophosphates is reported and it is shown that the technique can be employed for the study of open-framework catalytically active systems. Evidence that the cobalt ions on the surface of the crystals react differently to those in the bulk is found.

Keywords: EXAFS; energy-resolved electron-yield XAS; aluminophosphates; catalysis.

1. Introduction

The X-ray absorption spectroscopy (XAS) technique in the photon energy range from 4 to 40 keV (hard X-rays) is widely used to probe the local structure of active metal species in heterogeneous catalysts (Greegor & Lytle, 1980; Martis *et al.*, 2012; Rønning *et al.*, 2010; Tsakoumis *et al.*, 2012, 2013). It can render local structure information about metal species even if only present in low concentrations. It is suitable for structural studies under 'operando' conditions, while samples undergo chemical reactions at the desired temperatures and pressures (Beale *et al.*, 2005; Nagai *et al.*, 2013; Newton & van Beek, 2010). The main drawback with the conventional measurements (either in transmission or in fluorescence mode) of catalysts is that they provide more bulk information than near-surface information, due to the penetration of the hard X-rays, which is important in understanding catalytic materials. At energies lower than 4 keV, soft X-rays (in the photon range 0.1–1 keV) are particularly well suited for studying the electronic structure of a reacting catalyst surface because its surface sensitivity is naturally given by the lower energy of the Auger electrons after core hole excitation.

Surface and near-surface structure, as well as the oxidation state of metal ions, are important parameters related to catalytic activity and selectivity of materials. Relevant information can be obtained using surface-sensitive techniques like X-ray photoelectron spectroscopy and Auger electron spectroscopy (Ertl & Kuppers, 1985). However, these two techniques require samples to be kept under vacuum and thus prohibit operando heterogeneous catalysis experiments. In addition, the information is limited only to the chemical states of metal species. To circumvent this problem one can apply grazing-incidence XAS (GIXAS) (Floriano *et al.*, 2000) or total-electron-yield (Erbil *et al.*, 1988) XAS which can provide both structural and chemical information on the surface layers of the material. However, these techniques do not render depth-resolved information and are limited to thin films studies. This problem is shared by conventional electron-yield XAS where the samples should be contained under high-vacuum conditions due to the limited path length of electrons in the solid state or a gas.

Energy-resolved electron-yield X-ray absorption spectroscopy (EREY–XAS) was developed by Rayment *et al.* (2000). In this technique, electron-yield experiments in the photon energy range 4–20 keV are performed, but the active surface is exposed to a gaseous medium which acts as the electron amplification medium required for the operation of a gas microstrip detector (GMSD) which has the capability to detect Auger electrons in an energy-resolved mode. In these experiments the difference between the bulk and surface structure of the NiO/Ni model system was studied. However, this technique is in principle also suitable for the study of catalytic processes. In catalysis experiments the gas can serve the dual purpose of being the reaction gas as well as the electron amplification medium required for the GMSD. As an extra advantage, depth-resolved information can be obtained. The basic concept of the technique is that Auger electrons, which are emitted during the decay of the excited atomic states produced by X-ray absorption events, lose energy by various inelastic scattering processes (Erbil *et al.*, 1988). Since the number of loss events is related to the path length in the sample, then from the electron energy one can determine the depth below the surface where electrons have been generated (Chung & Jenkins, 1970; Larkins, 1977; Schroeder *et al.*,

1995*a*,*b*). Energy-selective detection of the electron-yield signal thus enables simultaneous recording of EREY–XAS from the 'high energy' region, *i.e.* Auger electrons escaping from the near-surface, and the 'low energy' region, for Auger electrons generated in the bulk of the material.

Typical escape depths of Auger electrons are between 100 and 1000 Å (Schroeder *et al.*, 1998), which defines the near-surface range over which useful information can be obtained (Abbey *et al.*, 2006; Vollmer *et al.*, 2003, 2004). To demonstrate the potential of EREY–XAS in catalysis research and enhance its application to nanoporous materials, we used it to determine the differences between the bulk and the near-surface activity of cobalt aluminophosphates (CoAlPOs). These systems are an important class of nanoporous materials because of their promising role in a range of catalytic reactions; for example, the selective conversion of methanol to light olefins and selective oxidation of alkane molecules in the presence of molecular oxygen (Chen & Thomas, 1994; Thomas *et al.*, 1999). Although the CoAlPOs catalysts have been extensively studied in the past for their catalytic potential, there are discrepancies in the literature regarding the nature and location of the Co^{2+} ions incorporated into the framework sites of AlPO molecular sieves (Weckhuysen *et al.*, 1999; Lohse *et al.*, 1997; Hartmann & Kevan, 2002). Although there is sufficient evidence to support an argument for the true isomorphous substitution of Co^{2+} ions, depending on the preparation methods and the nature of synthesis, extra-framework cobalt ions may be present. Even with the best synthesis methods there may be cobalt ions residing on the surface of the crystal (isomorphous substituted ones) which may be able to coordinate with other molecules (for example, water molecules) and these surface-substituted atoms may not contribute to the shape-selective catalysis. For good molecular shape selective catalysts it is important that these active sites are located inside the pores. Therefore, the structural and electronic differences in the surface (the top layer of ~50 Å) and near-surface region (50–100 Å) can play an important role in understanding the relationship between structure and catalytic properties. Although, a range of bulk spectroscopic techniques (Simmance *et al.*, 2009; Sankar & Raja, 2003; Sankar *et al.*, 1998, 2003, 2007; Barrett *et al.*, 1996) including XAS have been employed, a full description of the catalyst structure, particularly from the near-surface region, is still lacking.

The aim of this work is to employ EREY–XAS to determine the differences between the bulk and near-surface of CoAlPO catalysts. A test case for the usefulness of the technique is that it is possible to distinguish between framework and extra-framework Co^{2+} ions residing on the outer surface of the crystals. EREY–XAS bulk structural data are compared with that of transmission XAS data, which is dominated by the bulk structure, in order to validate structural data.

2. Experimental

A detailed description of the catalyst preparation is described elsewhere (Chen *et al.*, 1994; Chen & Thomas, 1994; Sankar *et al.*, 2003). CoAlPO-18 was prepared using *N*,*N*-diisopropylethylamine (DIPE) as the structure directing agent. The relative molar composition of the gel was calculated employing the formula $0.9\ Al^{3+}:0.1\ Co^{2+}:1P^{5+}:0.8$ DIPE: $25\ H_2O$, where cobalt acetate was used as a Co^{2+} source. The initial gel was prepared by dissolving aluminium hydroxide hydrate [$Al(OH)_3.xH_2O$; Sigma-Aldrich] in a solution of phosphoric acid (H_3PO_4, 85%; Sigma-Aldrich) with deionized water. An aqueous solution of cobalt(II) acetate tetrahydrate [$(CH_3COO)_2Co{\cdot}4\ H_2O$, 98%; Sigma-Aldrich] was then added to the mixture. After rigorously stirring the gel for 2 h, *N*,*N*-diisopropylethylamine {$[(CH_3)_2CH]_2NC_2H_5$, 99.5%; Sigma-Aldrich} was added to form the final gel which was stirred for several hours. The gel was then placed in an autoclave and heated at 433 K for four days.

CoAlPO-34 samples were prepared using tetraethylammonium hydroxide (TEAOH) as SDA (Lok *et al.*, 1984). The relative molar composition of gels used in this study was calculated employing the formula $0.9\ Al^{3+}:0.1\ Co^{2+}:1\ P^{5+}:$ x TEAOH:$25\ H_2O$, where x = 0.8 and 1. The samples were then heated at 443 K for three days.

The resulting solids were washed with distilled water, filtered and dried overnight at 373 K.

2.1. Transmission and energy-resolved electron-yield XAS

Co *K*-edge EREY and transmission XAS spectra were collected on the Dutch Belgium beamline (BM26A) (Nikitenko *et al.*, 2008) at the ESRF with the synchrotron ring operating in four-bunch mode giving ~40 mA electron current at 6 GeV energy. Room-temperature transmission XAS data were acquired in step scans over a k range from 3 to 12 $Å^{-1}$ using k^3-weighting for the counting time per data point increasing from 1 s at 3 $Å^{-1}$ to 5 s at 12 $Å^{-1}$. A full XAS spectrum was collected in ~34 min. In a typical experiment, the sample was pressed into a 13 mm pellet and fixed onto a sample holder.

The Co *K*-edge EREY–XAS were measured using the GMSD (Oed, 1988) which is housed in a custom-made chamber, *i.e.* e-yield detector. The GMSD consists of a glass plate lithographed with a pattern of 10 µm-wide anode strips interleaved with 90 µm-wide cathode strips, with a pitch of 300 µm. The e-yield detector was operating with a gas mixture of 10% isobutene and 90% helium, a drift voltage of −1500 V, cathode potential of −550 V and a grounded anode. A constant flow of 100 ml min^{-1} isobutene/He mixture was maintained through the vessel. The GMSD acts as anode, while the sample is the internal photocathode, as shown in Fig. 1. In order to minimize the sensitivity of the GMSD to electrons generated by X-ray interactions with the fill gas, the gas is chosen to have very long X-ray interaction lengths. The collected data are thus dominated by the electrons released from the sample. These electrons are drawn to the detector structure by the presence of an electric field and amplified by the gas gain as the GMSD is operated in its proportional region. The resulting charge avalanche is processed by an analogue signal chain consisting of a charge-sensitive pre-

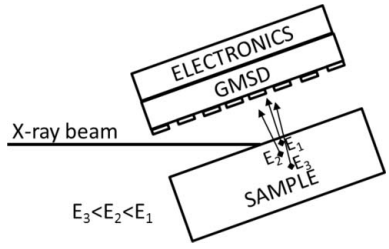

Figure 1
Detection of Auger electrons using the GMSD under ambient conditions after irradiating the sample with a direct X-ray beam, where E is the energy of the electrons escaping from the sample surface and/or bulk into the ambient gaseous environment. The electron escape energy is a function of the depth at which these have been generated. The larger the depth, the more loss events will take place. The sample bias is set to a high negative potential which creates the drift field accelerating the electrons towards the GMSD. The emergent electron energy profile (as shown in Fig. 2) contains information about the structure as a function of depth from the surface.

amplifier coupled to a shaping amplifier. The amplitude of the resulting spectra is thus proportional to the energy of the electron being analysed and is measured by a Fast ComTec 7072. A large number of events are processed in such a manner and the amplitudes are histogrammed by the readout system. These histograms are recorded as an ASCII file, *i.e.* Auger electron spectra. An example of a typical energy electron spectrum is shown in Fig. 2.

CoAlPO samples were sprinkled on a conductive carbon tape that was stuck onto flat metal plates made of brass, aluminium or copper. The flat plate with deposited sample was then positioned such that the beam was striking it under an angle of 2.5°. The GMSD sensor was mounted parallel to this.

In our experiments, we have used a gas mixture which is well characterized in GMSD operation. However, it is possible to use the detector with different gas mixtures which are relevant in catalysis research. The results of the investigation of the behaviour of the detector with various gas mixtures were reported by Vollmet *et al.* (2003). Gases are supplied to the detector using a custom-built gas rig consisting of four Brooks mass flow controllers (MFCs) with an accuracy given as 1% and a repeatability of 0.25% of the flow. The MFCs are fed into a gas-mixing manifold.

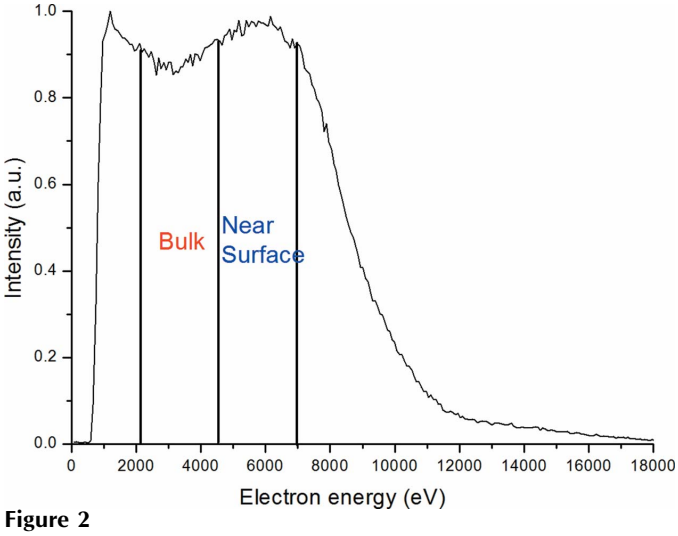

Figure 2
Auger electron spectrum obtained at a photon energy of 7903 eV from CoAlPO-34 A. Two different energy windows for Auger electron spectra for each primary photon beam are indicated. The decision about the number and width of energy windows is based on the quality of data, *i.e.* signal-to-noise ratio and objectives of the study, for instance, the depth profiling of the sample. The low-energy region is the Auger electrons which escape from the bulk, whereas the higher-energy electrons emanate from the near-surface region of the sample.

The EREY–XAS data were recorded using the e-yield detector over a similar k range as was used in the transmission XAS experiments. The sample was set at an inclination of 2.5° with respect to the X-ray beam. The horizontal and vertical size of the beam was 4 and 0.7 mm, respectively, and produced a beam footprint on the sample covering an area of $\sim$80 mm^2. In order to maintain the count rate below the detector saturation level, the beam intensity was, when required, attenuated by placing aluminium sheets before the sample. Auger electron spectra as a function of primary beam photon energy during the energy scan of the monochromator were measured. Auger electron spectra were collected with just two electron energy detection windows: a high-energy window for Auger electrons escaping close to the surface and low-energy window for Auger electrons from the bulk, as shown in Fig. 2. From Auger electron spectra were obtained a two-dimensional matrix, which contained information about the Auger electron spectrum at each photon energy. The integration of the two-dimensional matrix data within selected energy windows yielded EREY–XAS which were obtained by summing all Auger electron spectra. This was performed in a customized post-processing software package (*Reduce*) which was written in order to allow for a rapid data reduction process. The resulting EREY–XAS data can subsequently be analysed using standard available XAS software.

2.2. XAS and EREY–XAS data analysis

Transmission XAS as well as EREY–XAS data were normalized using *Athena* (Ravel & Newville, 2005). The non-linear least-squares fittings of extended X-ray absorption fine structure (EXAFS) and EREY–EXAFS data were performed using *EXCURVE98* (Binsted & Hasnain, 1996). The EXAFS and EREY–EXAFS data were analysed using the single scattering wave approximation (Gurman *et al.*, 1984). Phase shift and backscattering factors were calculated from atomic potentials using *EXCURVE98*. The non-structural parameter AFAC (the amplitude reduction due to many electron processes) was taken from the best fit to transmission EXAFS from Co foil and fixed at 0.85. During the refinement the coordination numbers were fixed to the crystallographic values. The same value of AFAC was used for EREY–EXAFS analysis. The refinement of transmission EXAFS data was carried out with k^3-weighting in the range 3.3–12.8 Å^{-1}. The refinement of EREY–EXAFS data was carried out with k^3-weighting in the range 3.3–8.5 Å^{-1}.

Although the EREY–EXAFS data k-range is shorter and therefore has a limited number of independent data points (Stern, 1993), N_I, it is still sufficient for fitting the first oxygen

shell. N_I defines the number of parameters that can be reliably obtained from the fitting of the EXAFS spectrum. In the case of transmission EXAFS data, the analyses were only performed on the first shell, since the primary aim of this work is to understand the immediate local environment around cobalt in the bulk and near-surface. It is also more practical for comparison of transmission EXAFS with that of EREY–EXAFS. During the refinement the coordination numbers were fixed to crystallographic values; however, bond distances and Debye–Waller factors were allowed to vary.

3. Results and discussion

XANES spectra can be used to distinguish between framework and extra-framework Co^{2+} species in CoAlPO samples. From previous work on cobalt-substituted aluminophosphates it is known that Co^{2+} species can be either incorporated into the framework in a tetrahedral coordination or be present as extra-framework ions in octahedral coordination (Barrett *et al.*, 1995, 1997). Accordingly, cobalt acetate ($C_4H_6CoO_4$) and cobalt aluminate ($CoAl_2O_4$), representing Co^{2+} in octahedral and tetrahedral environments, respectively, were chosen as reference materials (Dimitrou *et al.*, 1993; Greenwald *et al.*, 1954; McClure, 1957; van Niekerk & Schoening, 1953). Co *K*-edge XANES spectra of the reference materials are shown in Fig. 3. The Co^{2+} ions are tetrahedrally coordinated in $CoAl_2O_4$ (Toriumi *et al.*, 1978), and the XANES spectrum shows a pre-edge peak at ∼7708 eV. This latter feature is due to the 1*s* to 3*d* electronic transition which occurs during relaxation in the non-centrosymmetric environment, in which *d* and *p* Co—O molecular orbitals are mixed together (Kraushaar-Czarnetzki *et al.*, 1991; Moen *et al.*, 1997; Montes *et al.*, 1990). The transition is much stronger for Co^{2+} in the tetrahedral environment compared with that of octahedral coordination (Moen *et al.*, 1997) (see Fig. 3). Strong white line intensity (main edge intensity at ∼7722 eV) arises due to linear O—Co—O bonds from the 1*s* to 4*p* absorption transition.

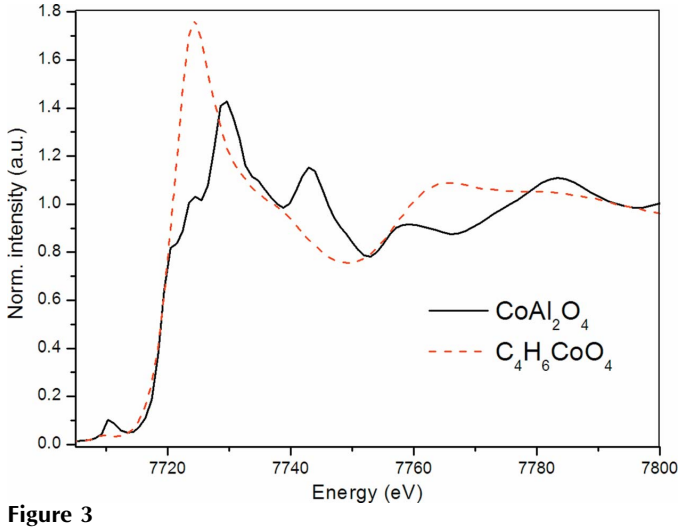

Figure 3
Comparison of Co *K*-edge XANES of $CoAl_2O_4$ and $C_4H_6CoO_4$ representing Co^{2+} ions in tetrahedral and octahedral coordination, respectively. There is a small pre-edge peak, due to the 1*s* to 3*d* electronic transition which is typical for tetrahedrally coordinated Co^{2+} ions. The XANES spectrum of octahedrally coordinated Co^{2+} ions shows strong white line intensity, while the pre-edge peak is absent.

Co *K*-edge EREY–XANES obtained from the near-surface and bulk as well as transmission XANES spectra of the as-prepared CoAlPO-34 A and B samples along with CoAlPO-18 are shown in Fig. 4. Comparison of bulk EREY–XANES with those of transmission XANES spectra indicates that the data are in agreement in terms of the reproducibility of XAS features. Transmission Co *K*-edge XANES of all three CoAlPO catalysts are identical. Their comparison with $CoAl_2O_4$ suggest that on average the arrangement of Co^{2+} ions in the catalysts is similar to $CoAl_2O_4$ in terms of local structure. The pre- and main-edge peak positions match well $CoAl_2O_4$. This indicates the presence of Co^{2+} ions in the tetrahedral sites in the framework of the material according to bulk XANES measurements. Similar results were found for Co *K*-edge EREY–XANES corresponding to the near-surface and bulk of CoAlPO-18, CoAlPO-34 A and B, which confirmed the uniform distribution of tetrahedrally coordinated Co^{2+} species between the bulk and near-surface sites.

In order to quantitatively determine structural parameters of the cobalt environment transmission Co *K*-edge EXAFS data of the model compounds, tetrahedral Co^{2+} in $CoAl_2O_4$ (Toriumi *et al.*, 1978) and octahedral Co^{2+} in $C_4H_6CoO_4$ were analysed (van Niekerk & Schoening, 1953). In $CoAl_2O_4$ (Barrett *et al.*, 1995) the Co^{2+} ions are surrounded by four tetrahedrally spaced oxygen atoms at 1.94 ± 0.01 Å. In $C_4H_6CoO_4$ the Co^{2+} ions are surrounded by six octahedrally arranged oxygen atoms at 2.08 ± 0.005 Å. Based on EXAFS data collected in transmission mode, the local structure around the cobalt atom in CoAlPO-34 A and B samples along with CoAlPO-18 can be accurately described by four tetrahedrally spaced oxygen atoms at a distance of 1.94 ± 0.003 Å. This bond distance, typical for Co^{2+} in tetrahedral environment, is in good agreement with values found in $CoAl_2O_4$ and the literature (Sankar *et al.*, 2003). The results are summarized in Table 1.

The EREY–EXAFS results for CoAlPO-34 A and B also rendered evidence for a tetrahedral environment. This indicates that the presence of extra-framework Co^{2+} species in the near-surface region of the catalysts can be ruled out. All Co^{2+} ions are located in the framework exclusively at tetrahedral sites, corroborating the XANES results. Changes in the Al/P ratios for these two samples did not have an influence on the incorporation of Co^{2+} ions into the framework. Typical fits to room-temperature Co *K*-edge transmission and EREY–EXAFS spectra of the as-prepared CoAlPO-34 and the associated Fourier transforms are shown in Fig. 5. In the figure we observe that EREY–EXAFS amplitudes are comparable with those of transmission data. The EREY–EXAFS are noisier but the data quality is sufficient to perform an EXAFS analysis of the first neighbours. The results are summarized in Table 2.

EREY–EXAFS results for CoAlPO-18 found in the bulk and near-surface four Co–O bonds at 1.96 ± 0.01 Å and 1.97 ± 0.01 Å (see Table 2), respectively, are slightly higher than

Table 1
Structural parameters obtained from analysis of transmission Co *K*-edge EXAFS data for the as-prepared catalysts and model compounds, where *N* is the coordination number, *R* is the bond distance and 2σ the Debye–Waller factor.

Sample	Scatter	*N*	*R* (Å)	$2\sigma^2$ (Å)
CoAlPO-34 A	O	4	1.94 ± 0.003	0.01
CoAlPO-34 B	O	4	1.94 ± 0.003	0.01
CoAlPO-18	O	4	1.94 ± 0.003	0.012
$CoAl_2O_4$	O	4	1.94 ± 0.010	0.008
$C_4H_6CoO_4$	O	6	2.08 ± 0.005	0.0014

expected for tetrahedrally coordinated Co^{2+} ions; previous studies reported a bond distance of 1.93 Å (Barrett *et al.*, 1996). The bond distances obtained from EREY data for both surface and bulk of the catalyst are higher than those of the EXAFS data recorded in transmission mode (1.94 ± 0.003 Å, see Table 1). Interestingly, there are slight differences in the near-surface region between near-surface and bulk but the EXAFS results are very similar which suggests stronger disorder at the surface.

Comparing the near-surface EREY–XANES with transmission XAS data, we note that there is no significant change in the edge energy, which would suggest that the oxidation state of cobalt ions in bulk and surface are closely similar. The possible explanation for the increase in Co—O distance is likely to be due to the presence of extra-framework cobalt ions which can be introduced during the crystallization process of aluminophosphate networks (Grandjean *et al.*, 2005). This suggests that not all cobalt ions are incorporated into a tetrahedral ALPO-18 framework during synthesis or some of the surface cobalt ions are susceptible to a change in coordination. A similar phenomenon was observed in Co/MCM-41 synthesis (Jentys *et al.*, 1996).

These results demonstrate that EREY–XAS can be used to distinguish between the surface and bulk Co environment. Therefore this technique is a useful tool for investigating the near-surface structure of nanomaterials, if the characteristic photon energy of the atom of interest lies in the range between 4 and 20 keV, where the production of Auger electrons is maximized (Ertl & Kuppers, 1985). The major advantage is that one is not required to keep the samples in a high vacuum but can operate at elevated pressures where the gas has the dual function of being the reaction gas as well as the electron amplification medium.

In this work we have shown that this technique is well suited for studies beyond model systems and can be applied to catalytically relevant materials like zeolites doped with a small amount of transition metal ions. This makes the technique favourable for investigation of supported heterogeneous catalysts encompassing nano-sized metals or metal oxides (such as Ti, V, Cr, Fe, Ni, Co) dispersed on a flat substrate [*i.e.* Si(100), glass, metal] or an oxide support (Al_2O_3, SiO_2). It is especially promising that the gas used for electron avalanche

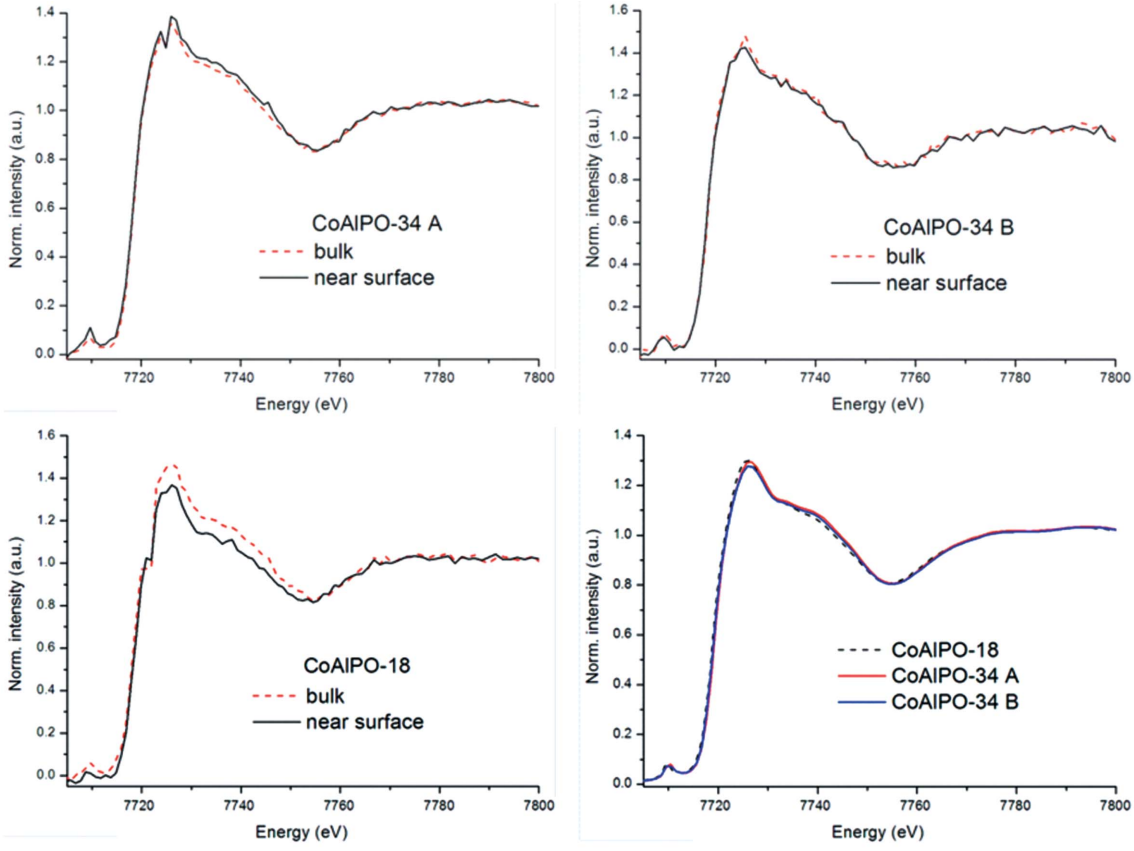

Figure 4
Co *K*-edge EREY–XANES for CoAlPO-34 A, CoAlPO-34 B and CoAlPO-18. The spectrum from the bulk is plotted in dashed red, whereas that from the near-surface is a solid black line. Transmission Co *K*-edge XANES of all catalysts are shown in the bottom right-hand corner. The XANES near-surface and bulk spectra exhibit a small pre-edge peak which is a characteristic of tetrahedrally coordinated Co^{2+} ions.

Table 2
Structural parameters obtained from the analysis of Co *K*-edge EREY–EXAFS data for as-prepared catalysts, where *N* is the coordination number, *R* is the bond distance and 2σ is the Debye–Waller factor.

Sample	Region	Scatter	*N*	*R* (Å)	$2\sigma^2$ (Å)
CoAlPO-34 A	Near-surface	O	4	1.94 ± 0.05	0.008
	Bulk	O	4	1.93 ± 0.05	0.006
CoAlPO-34 B	Near-surface	O	4	1.93 ± 0.05	0.01
	Bulk	O	4	1.94 ± 0.05	0.008
CoAlPO-18	Near-surface	O	4	1.96 ± 0.05	0.01
	Bulk	O	4	1.97 ± 0.05	0.01

amplification can be the same as the reactant gas in catalytic studies. For this, *in situ* EREY–XAS study (employing the e-detector) is essential, as it renders information from the region between the bulk and surface (100 and 1000 Å), whereby changes in the oxidation state of metal ions due to interaction with gas molecules during the reaction can be tracked. From a previous study on the GMSD and process gases it is known that the detector can operate not only with common reaction gases but it is also able to withstand water vapour and thus further broadens the range of chemical reactions that can be

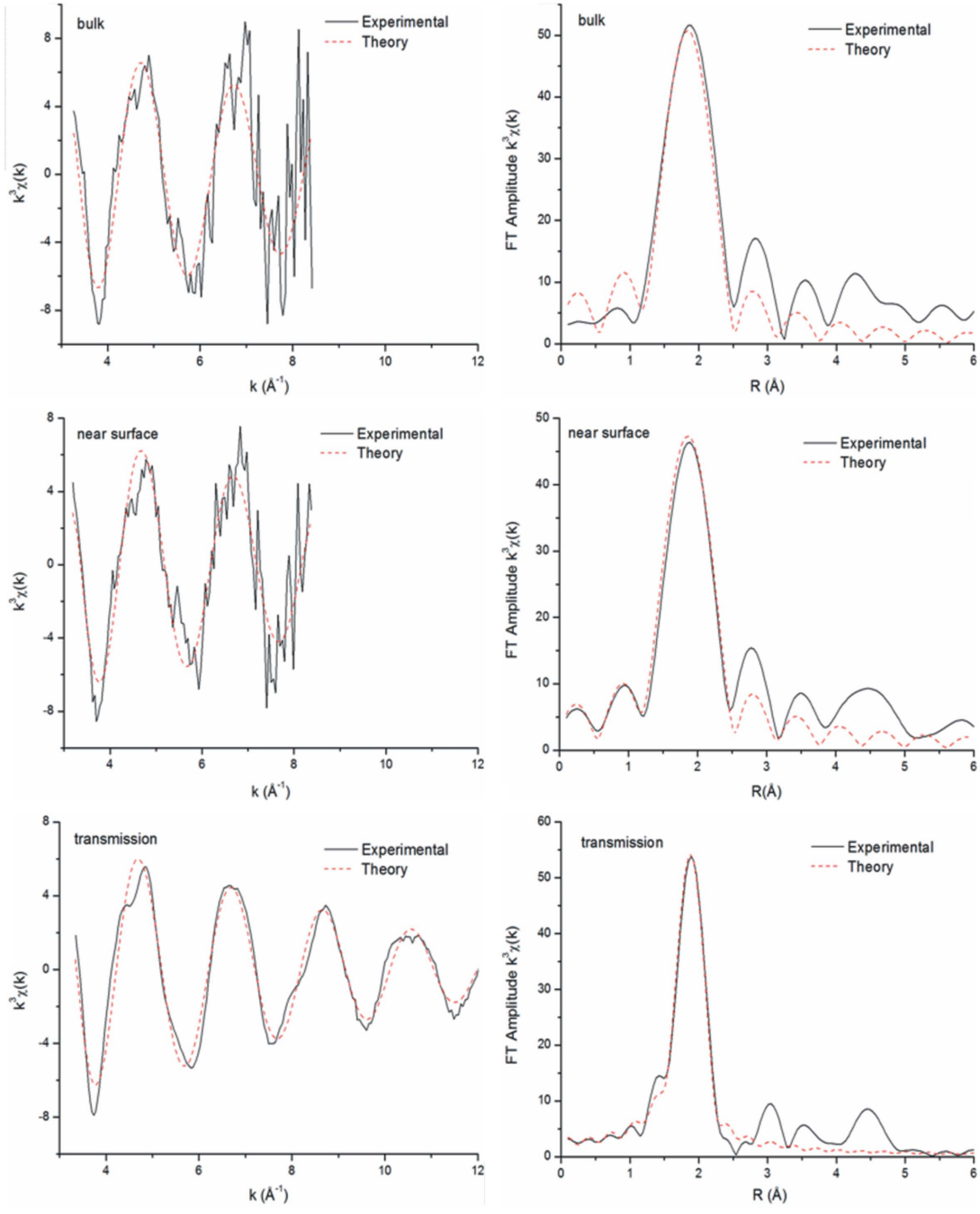

Figure 5
Comparison of Co *K*-edge EREY and transmission EXAFS together with corresponding Fourier transforms for CoAlPO-34 A. Data were analysed in *k*-space (after background subtraction, k^3-weighted). The solid line is the experimental data and the dashed line is the best fit. The EREY–EXAFS amplitudes are comparable with those of transmission EXAFS. The EREY–EXAFS spectra are noisier, particularly at higher *k*-values, but the data quality is sufficient for a full EXAFS analysis.

studied (Vollmer *et al.*, 2003). The operation of the detector with water vapour, for instance, enables electrochemistry or corrosions studies on materials under operando conditions.

The EREY–XAS data quality could be further improved by including an additional four data channels from the GMSD in the counting electronics.

4. Conclusion

The work described here shows that EREY–XAS is a useful technique for near-surface studies of catalytically relevant materials under ambient conditions, as it renders the near-surface information on chemical state as well as the local structure. It is also suitable for *in situ* operando studies of heterogeneous catalysts supported on metal oxides or flat plates. Lastly, we have shown that EREY–XAS can provide direct evidence about the incorporation of Co^{2+} ions into AlPOs frameworks.

The Netherlands Organization for Scientific Research is acknowledged for the use of facilities at beamline BM26A at the ESRF. The staff at BM26A are gratefully acknowledged for their help.

References

Abbey, B., Lipp, J. D., Barber, Z. H. & Rayment, T. (2006). *J. Appl. Phys.* **99**, 124914.

Barrett, P. A., Sankar, G., Catlow, C. R. A. & Thomas, J. M. (1996). *J. Phys. Chem.* **100**, 8977–8985.

Barrett, P. A., Sankar, G., Jones, R. H., Catlow, C. R. A. & Thomas, J. M. (1997). *J. Phys. Chem. B*, **101**, 9555–9562.

Barrett, P. A., Sankar, G., Richard, C., Catlow, A. & Thomas, J. M. (1995). *J. Phys. Chem. Solids*, **56**, 1395–1405.

Beale, A. M., van der Eerden, A. M. J., Kervinen, K., Newton, M. A. & Weckhuysen, B. M. (2005). *Chem. Commun.* pp. 3015–3017.

Binsted, N. & Hasnain, S. S. (1996). *J. Synchrotron Rad.* **3**, 185–196.

Chen, J. & Thomas, J. M. (1994). *J. Chem. Soc. Chem. Commun.* pp. 603–604.

Chen, J., Wright, P. A., Thomas, J. M., Natarajan, S., Marchese, L., Bradley, S. M., Sankar, G., Catlow, C. R. A. & Gai-Boyes, P. L. (1994). *J. Phys. Chem.* **98**, 10216–10224.

Chung, M. F. & Jenkins, L. H. (1970). *Surf. Sci.* **22**, 479–485.

Dimitrou, K., Folting, K., Streib, W. E. & Christou, G. (1993). *J. Am. Chem. Soc.* **115**, 6432–6433.

Erbil, A., Cargill III, G., Frahm, R. & Boehme, R. (1988). *Phys. Rev. B*, **37**, 2450–2464.

Ertl, G. & Kuppers, J. (1985). *Low Energy Electrons and Surface Chemistry*. Weinheim: VCH.

Floriano, P. N., Schlieben, O., Doomes, E. E., Klein, I., Janssen, J., Hormes, J., Poliakoff, E. D. & McCarley, R. L. (2000). *Chem. Phys. Lett.* **321**, 175–181.

Grandjean, D., Beale, A. M., Petukhov, A. V. & Weckhuysen, B. M. (2005). *J. Am. Chem. Soc.* **127**, 14454–14465.

Greegor, R. B. & Lytle, F. W. (1980). *J. Catal.* **63**, 476–486.

Greenwald, S., Pickart, S. J. & Grannis, F. H. (1954). *J. Chem. Phys.* **22**, 1597–1600.

Gurman, S. J., Binsted, N. & Ross, I. (1984). *J. Phys. Solid State Phys.* **17**, 143–151.

Hartmann, M. & Kevan, L. (2002). *Res. Chem. Intermed.* **28**, 625–695.

Jentys, A., Pham, N. H., Vinek, H., Englisch, M. & Lercher, J. A. (1996). *Microporous Mater.* **6**, 13–17.

Kraushaar-Czarnetzki, B., Hoogervorst, W. G. M., Andréa, R. R., Emeis, C. A. & Stork, W. H. J. (1991). *J. Chem. Soc. Faraday Trans.* **87**, 891.

Larkins, F. P. (1977). *At. Data Nucl. Data Tables*, **20**, 311–387.

Lohse, U., Parlitz, B., Müller, D., Schreier, E., Bertram, R. & Fricke, R. (1997). *Microporous Mater.* **12**, 39–49.

Lok, B. M., Messina, C. A., Patton, R. L., Gajek, R. T., Cannan, T. R. & Flanigen, E. M. (1984). *J. Am. Chem. Soc.* **106**, 6092–6093.

McClure, D. S. (1957). *J. Phys. Chem. Solids*, **3**, 311–317.

Martis, V., Oldman, R., Anderson, R., Fowles, M., Hyde, T., Smith, R., Nikitenko, S., Bras, W. & Sankar, G. (2012). *Phys. Chem. Chem. Phys.* **15**, 168–175.

Moen, A., Nicholson, D. G., Rønning, M., Lamble, G. M., Lee, J.-F. & Emerich, H. (1997). *J. Chem. Soc. Faraday Trans.* **93**, 4071–4077.

Montes, C., Davis, M. E., Murray, B. & Narayana, M. (1990). *J. Phys. Chem.* **94**, 6425–6430.

Nagai, Y., Dohmae, K., Nishimura, Y. F., Kato, H., Hirata, H. & Takahashi, N. (2013). *Phys. Chem. Chem. Phys.* **15**, 8461–8465.

Newton, M. A. & van Beek, W. (2010). *Chem. Soc. Rev.* **39**, 4845–4863.

Niekerk, J. N. van & Schoening, F. R. L. (1953). *Acta Cryst.* **6**, 609–612.

Nikitenko, S., Beale, A. M., van der Eerden, A. M. J., Jacques, S. D. M., Leynaud, O., O'Brien, M. G., Detollenaere, D., Kaptein, R., Weckhuysen, B. M. & Bras, W. (2008). *J. Synchrotron Rad.* **15**, 632–640.

Oed, A. (1988). *Nucl. Instrum. Methods Phys. Res. A*, **263**, 351–359.

Ravel, B. & Newville, M. (2005). *J. Synchrotron Rad.* **12**, 537–541.

Rayment, T., Schroeder, S. L. M., Moggridge, G. D., Bateman, J. E., Derbyshire, G. E. & Stephenson, R. (2000). *Rev. Sci. Instrum.* **71**, 3640.

Rønning, M., Tsakoumis, N. E., Voronov, A., Johnsen, R. E., Norby, P., van Beek, W., Borg, Ø., Rytter, E. & Holmen, A. (2010). *Catal. Today*, **155**, 289–295.

Sankar, G., Fiddy, S., Beale, A. M., Harvey, I., Hayama, S. & Bushnell-Wye, G. (2007). *AIP Conf. Proc.* **882**, 585–587.

Sankar, G. & Raja, R. (2003). *Nanostructured Catalysts*, edited by S. L. Scott, C. M. Crudden and C. W. Jones, pp. 195–212. New York: Springer (ISBN 978-0-387-30641-4).

Sankar, G., Raja, R. & Thomas, J. M. (1998). *Catal. Lett.* **55**, 15–23.

Sankar, G., Wyles, J. K. & Catlow, C. R. A. (2003). *Top. Catal.* **24**, 173–184.

Schroeder, S. L. M., Moggridge, G. D., Lambert, R. M. & Rayment, T. (1998). *Advances in Spectroscopy*, Vol. 26, *Spectroscopy for Surface Science*, edited by, R. J. H. Clark and R. E. Hester, pp. 1–29. Chichester: John Wiley and Sons.

Schroeder, S. L. M., Moggridge, G. D., Ormerod, R. M., Lambert, R. M. & Rayment, T. (1995*b*). *Physica B*, **208–209**, 215–216.

Schroeder, S. L. M., Moggridge, G. D., Ormerod, R. M., Rayment, T. & Lambert, R. M. (1995*a*). *Surf. Sci.* **324**, L371–L377.

Simmance, K., Sankar, G., Bell, R. G., Prestipino, C. & van Beek, W. (2009). *Phys. Chem. Chem. Phys.* **12**, 559–562.

Stern, E. A. (1993). *Phys. Rev. B*, **48**, 9825–9827.

Thomas, J. M., Raja, R., Sankar, G. & Bell, R. G. (1999). *Nature (London)*, **398**, 227–230.

Toriumi, K., Ozima, M., Akaogi, M. & Saito, Y. (1978). *Acta Cryst.* B**34**, 1093–1096.

Tsakoumis, N. E., Dehghan, R., Johnsen, R. E., Voronov, A., van Beek, W., Walmsley, J. C., Borg, Ø., Rytter, E., Chen, D., Rønning, M. & Holmen, A. (2013). *Catal. Today*, **205**, 86–93.

Tsakoumis, N. E., Voronov, A., Rønning, M., Beek, W., v, Borg, Ø., Rytter, E. & Holmen, A. (2012). *J. Catal.* **291**, 138–148.

Vollmer, A., Lipp, J. D., Lee, J. R. I., Derbyshire, G. E. & Rayment, T. (2003). *Anal. Chem.* **75**, 6571–6575.

Vollmer, A., Lipp, J. D., Weiss, H., O'Malley, R. & Rayment, T. (2004). *Angew. Chem. Int. Ed.* **43**, 3691–3695.

Weckhuysen, B. M., Rao, R. R. A., Martens, J. & Schoonheydt, R. A. (1999). *Eur. J. Inorg. Chem.* **1999**, 565–577.